Shigella generates distinct IAM subpopulations during epithelial cell invasion to promote efficient intracellular niche formation

Lisa Sanchez, Arthur Lensen, Michael Connor, Mélanie Hamon, Jost Enninga, Camila Valenzuela

European Journal of Cell Biology 103 (2024) 151381

Contents lists available at ScienceDirect

European Journal of Cell Biology

journal homepage: www.elsevier.com/locate/ejcb

Shigella generates distinct IAM subpopulations during epithelial cell invasion to promote efficient intracellular niche formation

Lisa Sanchez [a,1], Arthur Lensen [a,1], Michael G. Connor [b], Mélanie Hamon [b], Jost Enninga [a,*], Camila Valenzuela [a,*]

[a] Institut Pasteur, Université Paris Cité, CNRS UMR3691, Dynamics of Host-Pathogen Interactions Unit, 75015 Paris, France
[b] Institut Pasteur, Université Paris Cité, Chromatin and Infection Unit, 75015 Paris, France

ARTICLE INFO

Keywords:
Bacterial invasion
Shigella flexneri
BAR domain-containing protein
Intracellular lifestyle
Endosomal recycling

ABSTRACT

The facultative intracellular pathogen *Shigella flexneri* invades non-phagocytic epithelial gut cells. Through a syringe-like apparatus called type 3 secretion system, it injects effector proteins into the host cell triggering actin rearrangements leading to its uptake within a tight vacuole, termed the bacterial-containing vacuole (BCV). Simultaneously, *Shigella* induces the formation of large vesicles around the entry site, which we refer to as infection-associated macropinosomes (IAMs). After entry, *Shigella* ruptures the BCV and escapes into the host cytosol by disassembling the BCV remnants. Previously, IAM formation has been shown to be required for efficient BCV escape, but the molecular events associated with BCV disassembly have remained unclear. To identify host components required for BCV disassembly, we performed a microscopy-based screen to monitor the recruitment of BAR domain-containing proteins, which are a family of host proteins involved in membrane shaping and sensing (e.g. endocytosis and recycling) during *Shigella* epithelial cell invasion. We identified endosomal recycling BAR protein Sorting Nexin-8 (SNX8) localized to IAMs in a PI(3)P-dependent manner before BCV disassembly. At least two distinct IAM subpopulations around the BCV were found, either being recycled back to cellular compartments such as the plasma membrane or transitioning to become RAB11A positive "contact-IAMs" involved in promoting BCV rupture. The IAM subpopulation duality was marked by the exclusive recruitment of either SNX8 or RAB11A. Hindering PI(3)P production at the IAMs led to an inhibition of SNX8 recruitment at these compartments and delayed both, the step of BCV rupture time and successful BCV disassembly. Finally, siRNA depletion of SNX8 accelerated BCV rupture and unpeeling of BCV remnants, indicating that SNX8 is involved in controlling the timing of the cytosolic release. Overall, our work sheds light on how *Shigella* establishes its intracellular niche through the subversion of a specific set of IAMs.

1. Introduction

The entero-invasive bacterial pathogen *Shigella flexneri* (hereafter referred to as *Shigella*) is the causative agent of bacillary dysentery which affects an estimated 80 to 165 million individuals annually (CDC, 2019) representing a major health threat (Mahbubur et al., 2007; Kim et al., 2008; Puzari et al., 2018). To invade non-phagocytic epithelial gut cells, *Shigella* uses a syringe-like apparatus termed the type 3 secretion system (T3SS) to reprogram the host actin cytoskeleton around the entry site (Schroeder and Hilbi, 2008, Valencia-Gallardo et al., 2014). This leads to the formation of positively shaped membranes ruffles whose collapse prompts the formation of concave membrane compartments. These enable (i) the internalization of the bacterium within a tight phagosome-like vacuole (Weiner et al., 2016) referred to as the bacteria-containing vacuole (BCV) and simultaneously (ii) the formation of vesicles heterogeneous in size and with a similar morphology to macropinosomes (Cossart and Sansonetti, 2004; Weiner et al., 2016), termed infection-associated macropinosomes (IAMs). *Shigella* then triggers BCV rupture and disassembly, prompting its access to the host cell cytosol where it replicates and spreads by forming an actin comet tail propelling it to adjacent cells (Cossart and Sansonetti, 2004; Kühn et al., 2020; Chang et al., 2020).

Although the contribution of host molecular pathways subverted in the invasion and niche establishment of intravacuolar bacterial

* Corresponding authors.
E-mail addresses: jost.enninga@pasteur.fr (J. Enninga), camila.valenzuela-montenegro@pasteur.fr (C. Valenzuela).
[1] These authors contributed equally.

https://doi.org/10.1016/j.ejcb.2023.151381
Received 22 May 2023; Received in revised form 20 December 2023; Accepted 24 December 2023
Available online 29 December 2023

pathogens is well-defined, it remains less clear for cytosol-residing bacteria (López-Montero and Enninga, 2016, Mellouk and Enninga, 2016). While BCV rupture has been suggested to be T3SS-mediated through the translocator proteins IpaB and IpaC (High et al., 1982, Blocker et al., 1999, Du et al., 2012), we previously demonstrated an impact of the endosomal recycling small GTPase RAB11A recruited to IAMs in promoting BCV rupture (Mellouk et al., 2014; Weiner et al., 2016). We furthermore reported that BCV damage is followed by membrane remnant disassembly, a process indispensable for *Shigella* cytosolic niche establishment (Kühn et al., 2020; Chang et al., 2020), in which membrane remnants in close proximity to the bacteria get actively removed. Membrane disassembly requires RAB8A and RAB11A to be recruited to IAMs and brought in proximity of the BCV by the exocyst complex (Chang et al., 2020). Combined, these findings demonstrate a need to comprehensively analyze the contribution of host trafficking factors in the context of *Shigella* invasion. Moreover, they depict IAMs not as bystander compartments but rather as main actors in the process of *Shigella* intracellular niche formation, highlighting the need to revisit and clarify the *Shigella* infection process.

Membrane remodeling is actively driven by a combination of local changes in membrane lipid composition and protein-generated membrane reshaping. This process drives the formation of a positive or a negative curvature necessary for several cellular processes from filopodia formation to endocytosis (McMahon and Gallop, 2005; Jarsch et al., 2016; Simunovic et al., 2019). Several bacterial invasion processes induce extensive host membrane reshaping by curving the membrane surrounding the entering bacteria prior to subsequent curvature collapse, as exemplified by membrane ruffling during *Shigella* entry (Swanson, 2008; Cossart and Roy, 2010; Ribet and Cossart, 2015; Buckley and King, 2017). Moreover, the formation of phagosomes and macropinosomes has also been shown to require extensive membrane reshaping (Swanson, 2008) for vesicle formation, scission and stability which all require changes in lipid composition as well as protein intervention (Swanson, 2008; Swanson, 2014).

BAR (Bin/Amphiphysin/Rvs) domain-containing proteins have been described as membrane-binding proteins specializing in membrane reshaping and curvature sensing (McMahon and Gallop, 2005, Allison Suarez et al., 2014, Simunovic et al., 2015, Simunovic et al., 2019). Characterized by the presence of a membrane-binding BAR domain, these proteins act in diverse cellular processes as signaling platforms (e.g. filopodia formation) and scaffolds (e.g. endosomal recycling) (Peter et al., 2004; Simunovic et al., 2015; Simunovic et al., 2019). Due to this, BAR domain proteins have been reportedly hijacked by invasive bacterial pathogens to facilitate their entry into the host cell. *Enterohemorrhagic E. coli* was reported to reprogram negative curvature-inducing and actin remodeling factor IRSp53 to form an actin structure called a pedestal (Weiss et al., 2009; Yi and Goldberg, 2009). Similarly, endosomal recycling BAR protein SNX1 is recruited to the *Salmonella*-containing vacuole through the bacterial effector SopB, to form tubular structures forming the *Salmonella* replicative niche (Bujny et al., 2008; Stévenin et al., 2019). In the case of *Shigella*, TOCA-1 has been shown to be implicated in actin rearrangements for the formation of an actin cocoon prior to BCV rupture, and is also present at actin tails (Leung et al., 2008; Baxt and Goldberg, 2014; Kühn et al., 2020).

Here, we exploited a high-content multidimensional time-resolved fluorescence microscopy assay (Sanchez et al., 2022) to screen a BAR protein library and comprehensively analyze their involvement during the successive *Shigella* invasion steps. Focusing on host factors possibly involved in BCV rupture, we identified the sorting nexin-BAR family member SNX8 to be strongly present at a subset of IAMs before BCV damage, and remaining there until membrane remnant disassembly. The characterization of the SNX8-positive IAM subset showed a distinct maturation from "canonical" macropinosomes. A large percentage of these IAMs were also positive for both PI(3)P, and the use of PI(3)P-kinase inhibitors led to delayed BCV rupture. Depleting SNX8 independently of the modulation of PI(3)P levels, led to a faster rupture and more efficient BCV disassembly. This indicated that SNX8-positive IAMs work in controlling the pace of BCV rupture, delaying the cytosolic escape of *Shigella* into the host cytosol. This diversity in IAMs reveals the *Shigella* invasion process as a complex sequence of events with the bacteria hijacking multiple pathways of the endocytic and recycling pathways for bacterial survival and cytosolic access.

2. Materials and methods

2.1. Bacterial strains and culture

In this study we used the *Shigella flexneri* strain M90T (Sansonetti et al., 1982) expressing the uropathogenic *E. coli* adhesin AfaI. Prior to infection experiments, *Shigella* strains were grown overnight at 37 °C from bacterial colonies grown on Trypticase Casein Soy Broth agar plates supplemented with ampicillin at 50 μg/mL and 0.01% Congo Red. Bacterial cultures were prepared by inoculating 3 colonies in TCSB media supplemented with ampicillin 50 μg/mL and incubated overnight at 37 °C, 220 rpm.

2.2. Cell lines and culture conditions

HeLa cervical adenocarcinoma CCL2 clone from the American Type Culture Collection (ATCC) and CaCo-2 TC7 cells (ATCC) were cultured in Dulbecco's Modified Eagle Medium (DMEM High glucose with GlutaMAX™ and pyruvate, Gibco, #31966–021) supplemented with 10% heat-inactivated Fetal Bovine Serum (Sigma Aldrich) and incubated at 37 °C, 5% CO_2.

2.3. Plasmids, cloning and cell line generation

The full list of plasmids used in this study is listed in Supplementary Table 1. The entire EGFP-tagged BAR domain plasmid library was a kind gift from Emmanuel Boucrot and is referenced in Chan Wah Hak et al. (2018). pDEST-SNX8-mApple was cloned by restriction enzyme digestion. Generation of stable HeLa cell lines was performed using the Sleeping Beauty System (Kowarz et al., 2015). We generated cell lines expressing fluorescent SNX8 and the plasma membrane marker LactC2 using pSBbi-Neo-SNX8-eGFP and pSBbi-Neo-LactC2-GFP. Both were cloned by in vivo assembly using SLIC (Jeong et al., 2012). JetPRIME (Polyplus, #101000027) was used to transfect plasmids into low passage HeLa cells with selection being performed using G418 at 800 ng/mL (Euromedex, #EU0601) for 7 days. The cells were then collected, and serial dilution was performed in a 96 well plate with maintenance of the selection pressure. The selected cells were then amplified and sorted based on their fluorescence level using a BD FACSAria™ III Cell Sorter. Live cells were gated in FSC-A/SSC-A and doublets were removed using the parameters FSC-A and FSC-H. Three populations, according to the GFP or EGFP intensities, were sorted as low-, medium- and high-expressing GFP/EGFP cells.

2.4. Cell seeding and transient transfections

Cells were seeded in either black 96-well plates (Greiner Bio-One, #655090) or in a 35 mm glass-bottom dish (ibiDI, #81158) containing a 4-chamber silicone insert (ibiDI, #80409). For both supports, HeLa cells were seeded at a density of 8000 cells per well, whereas CaCo-2 TC7 cells were seeded at a density of 5000 cells per well. Transient transfections were performed the following day by lipofection using FuGENE™ HD (Promega, #E2311) as instructed by the manufacturer. Briefly, transfection complexes were prepared by diluting 2 μg of plasmid (or for co-transfections, 1 μg of each plasmid) in 100 μL Opti-MEM (Gibco, #31985062), mixed with 4 μL of FuGENE™ HD and incubated for 10 min at room temperature. Afterwards, 5 μL of transfection mixture was added per well containing the cells seeded the

previous day, which were then incubated 48 h at 37 °C, 5% CO_2 prior to infection and imaging.

2.5. siRNA transfection

Cells were seeded in 35 mm glass-bottom dish (ibiDI, #81158) containing a 4-chamber silicone insert (ibiDI, #80409). siRNA transfection was performed at the same time as cell seeding using Lipofectamine RNAiMAX transfection reagent (Thermo Fisher) and Opti-MEM (Gibco, #31985–062). In brief, the sequence of siRNA for human SNX8 was obtained from MISSION (Sigma-Aldrich, #EHU048091), and the non-targeting siRNA control ON-TARGETplus was obtained from Dharmacon (GE Healthcare, # D-001810–10-05). Both siRNA were diluted at a final concentration of 100 nM and incubated with the cells for 72 h prior to infection. Knock-down efficiency was confirmed by real-time quantitative PCR and Western Blotting.

2.6. Infection protocol

Infections were carried out as previously described (Chang et al., 2020). Bacterial inoculum were prepared by diluting an overnight culture to 1:100 in 8 mL of fresh TCSB media supplemented with ampicillin 50 μg/mL and incubated for 2 h at 37 °C, 220 rpm. Once the subculture $OD_{600\ nm}$ reached 0.4–0.6, 1 mL of the subculture was spun 1 min at 6000 *g* and the bacteria pellet was washed twice with warm EM buffer (120 mM NaCl, 7 mM KCl, 1.8 mM $CaCl_2$, 0.8 mM $MgCl_2$, 5 mM glucose, 25 mM HEPES, pH 7.3). An inoculum was prepared by diluting the bacterial suspension in EM buffer to reach a multiplicity of infection (MOI) of 20 bacteria/cell. For inhibitor experiments, wortmannin (Sigma Aldrich, #W1628–1MG) and SAR405 (Selleckchem, #S7682) were diluted into the inoculum to 3.3 μm and 3 μM respectively from a DMSO stock solution. Prior to infection, the cells were washed three times with EM Buffer, and 50 μL of EM buffer were left in the well. For time lapse imaging experiments, the infection was started by adding 40 μL of inoculum per well in a 37 °C heated microscopy chamber and image acquisition was started. For endpoint experiments through cell fixation, no medium was left in the well and 30 μL of inoculum plus 0.5 mg/mL final dextran 10 000 MW Alexa-647 (Invitrogen™, #D22914) was added to the well, after which the samples were incubated at 20 °C for 10 min to enable the bacteria to reach the cells. Infection was then triggered by incubation at 37 °C for 30 min. Afterwards, samples were fixed using 4% paraformaldehyde (ThermoScientific, #043368.9 M) for 10 min at room temperature and washed 3 times with PBS.

2.7. Immunofluorescence

Following the fixation procedure, the cells were permeabilized using saponin diluted to 0.025% in PBS for 20 min at room temperature. Next, 3 PBS washes were performed and blocking was done with 2% Bovine Serum Albumin (Sigma Aldrich,#A7906–100 G) and 5% goat serum (Sigma Aldrich, #G9023) in PBS for 1 h at room temperature. Afterwards, rabbit anti-SNX8 primary antibody (Sigma Aldrich, #HPA057296) diluted at 1:250 in blocking solution was incubated on the sample 1 h at room temperature followed by a 45 min incubation of a goat anti-rabbit Alexa-488 secondary antibody (Invitrogen, #A11034) diluted to 1:500 together with Hoechst (Invitrogen, #1681305)and rhodamine-phalloidin (Invitrogen, #R415), according to the manufacturer instructions. Finally, cells were washed 3 times with PBS and left in PBS protected from the light until imaging.

2.8. Time lapse microscopy

The time-resolved BAR domain protein screen experiments were performed in a Nikon Ti-E inverted microscope equipped with a Perfect Focus System (TI-ND6-PFS Perfect Focus Unit) using a 40X/ 0.75 NA air objective. High spatio-temporal resolution time-lapses were acquired on DeltaVision Elite (Leica) using a 60X/1.42 NA oil objective with a 0.35 μm z-step and images were deconvolved using an integrated deconvolution software. Imaging of fixed experiments were acquired on a Nikon Ti-E inverted microscope equipped with a Perfect Focus System and a Yokogawa confocal spinning disk unit (CSU-W1) using a 60X/1.2 NA water objective. In this case, an automatic pipeline with autofocus using brightfield and Hoechst signal were used to define the focal plane of randomly generated positions. Images were acquired at a step-size of 0.5 μm in the z-plane.

2.9. Image processing and quantification

Images were processed using Fiji (https://imagej.net/software/fiji/, version 2.1.0/1.53c). For the BAR domain screen, BAR protein TOCA-1 and EGFP were used as positive and negative controls respectively (Leung et al., 2008; Kühn et al., 2020). Positive hits were counted as showing enrichment of the "candidate" proteins to the infection site by comparison to the EGFP control (see Fig. 1**B**). Quantification of SNX8 positive IAMs was done manually. Total dextran-labelled IAMs counting was performed by an automatic pipeline in Cell Profiler (www.cellprofiler.org, version 4.2.1). Briefly, regions of interest (ROIs, invasion foci) were determined by hand and cropped in every image. These ROIs were then processed by Fiji to perform a Sum-slice Z projection. In these processed ROIs, IAMs were then detected and counted using the dextran signal as well as a size threshold, allowing us to remove background noise.

2.10. Statistical analysis

Statistical analysis was performed using GraphPad Prism version 9.0.0 for MacOS, GraphPad Software, San Diego, California USA, www.graphpad.com.

3. Results

3.1. Identification of BAR domain-containing host factors enriched at Shigella invasion foci

With the aim of identifying new molecular pathways involved in the early steps of *Shigella* invasion of epithelial cells, we carried out a high-content time-resolved microscopy screen using a library of 66 EGFP-tagged full length BAR domain-containing proteins (see Supplementary Table 1 for full list). In parallel, we also followed the signals of fluorescently tagged Galectin-3, a cytosolic reporter that binds to the inner leaflet of the BCV membrane at the precise moment of vacuole rupture (Paz et al., 2010; Sanchez et al., 2022). In brief, a 2-minute-interval time-course of mOrange-Galectin-3 stably expressing HeLa cells transiently transfected with each plasmid from the BAR protein library and challenged with wildtype (WT) *Shigella* were recorded (Fig. 1**A**). This set-up enabled to track the BAR domain protein being recruited to the infection focus and simultaneously monitoring of 3 distinct *Shigella* invasion events: a) *Shigella*-triggered membrane ruffling, b) the step of BCV rupture, and c) the events of BCV membrane disassembly upon rupture. Candidate targets were scored against a positive recruitment control TOCA-1 (Leung et al., 2008; Kühn et al., 2020) and EGFP negative recruitment control. (Fig. 1**B**).

After manual inspection of the data based on the behavior of the external controls, 13 BAR domain-containing proteins were identified as positive hits (see Supplementary Table 2), whereas 10 were determined to be inconclusive due to poor transfection efficiency or low fluorescence signal and were removed from further analysis. Our results revealed specific subtypes of BAR domain-containing proteins localizing to different bacterial compartments. Among the hits were several members of the SNX-BAR family of proteins and actin nucleating factors such as Oligophrenin and PACSINs 1–3. We observed distinct recruitment patterns for these hit proteins during the infection. While PACSIN3

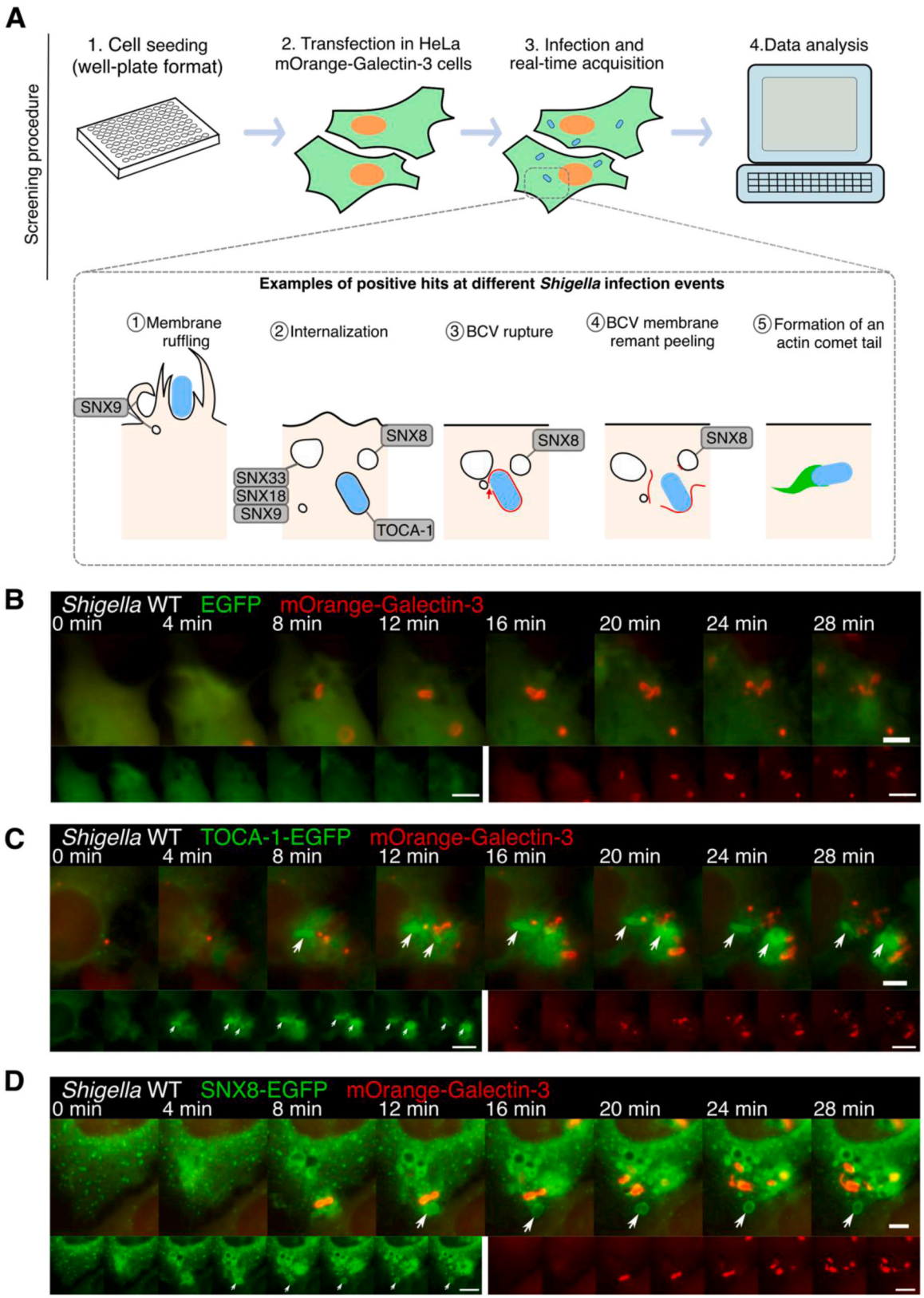

Fig. 1. Time-resolved high-content screen experimental procedure and examples of positive hits of host proteins recruited to the bacterial infection foci. A. Schematic illustration of the time-resolved screen workflow with examples of positive hits and their observed localization during *Shigella* infection events. HeLa mOrange-Galectin-3 cells were seeded, transfected with the proteins-of-interest and samples were infected with *Shigella* during microscopy acquisition. Examples of observed hit recruitment and their localization to the infection site are represented in the lower portion of the figure. **B. C. D.** Microscopy images of external controls EGFP and TOCA-1 as well as an example of positively identified hit: the SNX-BAR family SNX8 protein. In all figures, in red is shown the mOrange-Galectin-3 signal marking *Shigella*-BCV rupture and the BCV-membrane remnants, and in green the BAR-domain containing proteins included in the screen. White arrows show the recruitment of TOCA-1-EGFP to un-ruptured BCVs or SNX8 to IAMs. Scale bars are 5 μm and 10 μm.

recruitment was observed early during membrane ruffling, Oligophrenin was found to localize at the BCV prior to BCV rupture (Supplementary Figure 1). Interestingly, multiple members of the SNX-BAR family localized to IAMs early in their formation and/or their enrichment occurred throughout *Shigella* BCV egress (Fig. 1 and Supplementary Figure 1). Among them, we noticed a significant enrichment of the early endosome sorting protein Sorting Nexin 8 (SNX8) to IAMs (Fig. 1**D**). This recruitment was observed early on during the infection, and the protein remained persistently localized at the IAMs throughout the steps of *Shigella* BCV disassembly. Given the role of IAMs in BCV rupture and unpeeling, the persistent recruitment of SNX8 suggests it could be involved in several steps leading to cytosolic access.

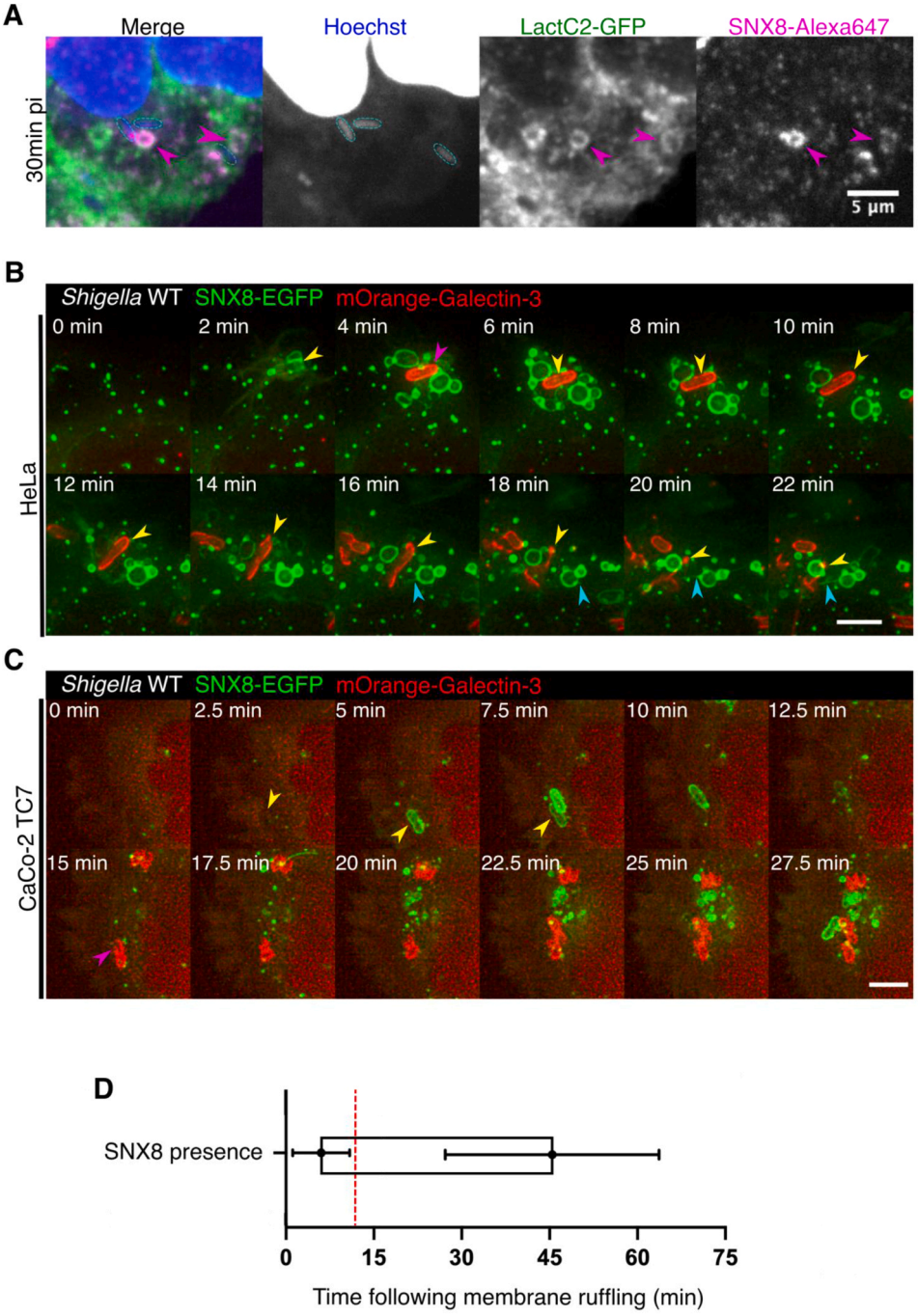

Fig. 2. SNX8 is recruited to IAMs and BCV prior to *Shigella*-BCV egress. A. Fixed confocal microscopy of LactC2-GFP stably expressing HeLa cells (in green) infected with *Shigella* for 30 min and stained for endogenous SNX8 (in magenta). The bacteria and cell nucleus were marked with Hoechst (in blue). Magenta arrowheads show individual IAMs recruiting endogenous SNX8 and bacteria are outlined in cyan. Scale bar: 5 µm. **B, C.** Time-lapse microscopy images of HeLa cells (B) and CaCo-2 cells (C) transfected with mOrange-Galectin-3 (in red) and SNX8-EGFP (in green) infected with *Shigella* WT. Yellow arrowheads point to an entering bacterium, magenta arrowheads indicate the moment of BCV rupture. Cyan arrows show multiple SNX8-positive tubules emerging from an individual SNX8-positive IAM. The infection start (t = 0) was defined by the first apparition of membrane ruffles. Scale bar: 3 µm. **D.** Quantitative analysis of SNX8-EGFP temporal recruitment sequence to the infection focus in HeLa cells expressing SNX8-EGFP and infected with *Shigella* WT. SNX8 presence is shown as a box with the average start of the recruitment at 6 min and dissipation at 44 min. Infection foci from two biological replicas were analyzed (n > 60). Bar shows the average start and end of SNX8 presence at the BCV + /- standard deviation. The red line represents the average BCV rupture time point (12 min).

3.2. SNX8 localizes to IAMs and the Shigella-BCV prior to BCV rupture and disassembly

SNX8 has been shown to localize to early endosomes and is suggested to recycle endocytic cargo to the Trans-Golgi network (Dyve et al., 2009). Although the function of human SNX8 remains elusive, its yeast homologue MVP1 has been shown to function in retromer-independent recycling (Suzuki et al., 2021). SNX8 has also been linked to several pathologies involving endosomal recycling defects such as Alzheimer's (Xie et al., 2019; Vanzo et al., 2014). With our identification of SNX8 localization and retention to IAMs we sought to define its functional contribution to *Shigella* entry.

Following the identification of SNX8 as a hit in our screen, we proceeded to comprehensively characterize SNX8 recruitment to IAMs. To rule out SNX8 recruitment to the BCV or IAMs due to ectopic expression artifacts we determined the localization of endogenous SNX8 by immunodetection using an anti-SNX8 antibody. Simultaneously, we used the previously described cellular imaging biosensor LactC2, which binds specifically to phosphatidylserine (Leung et al., 2008, Vecchio and Stahelin 2018) allowing us to monitor all of the plasma membrane-derived IAMs. Confocal microscopy analysis confirmed the presence of endogenous SNX8 to LactC2-marked vesicles in proximity to *Shigella* (Fig. 2**A**). We then assessed SNX8 behavior in relation to the ruptured BCV membrane. Temporal analysis of images from higher spatial resolution live-cell imaging (see methods for details) of HeLa and CaCo-2 cells transiently co-expressing SNX8-EGFP and mOrange-Galectin-3 showed the recruitment of SNX8 to *Shigella*-IAMs occurred prior to BCV rupture and remained at the IAMs until full cytosolic release of *Shigella* after BCV disassembly (Figs. 2**B** and 2**C**). Our results show SNX8 recruitment to the *Shigella* entry foci in HeLa cells roughly 6 min prior to BCV rupture and throughout BCV disassembly, which we previously showed occurs 20 min post-infection (Chang et al., 2020) (Fig. 2**D**). Moreover, SNX8 time-lapses showed SNX8 positive tubules emanating from IAMs (Fig. 2**B**), as previously described for SNX-BARs by Van Weering et al. (2010). We also observed the BCV to be transiently enriched in SNX8 prior to BCV rupture (Fig. 2**B**). Altogether, these results temporally map SNX8 recruitment to IAMs at early steps of BCV rupture and/or disassembly.

3.3. SNX8 recruitment is partially-driven by Shigella bacterial effectors IpgD and IcsB

Our data demonstrated SNX8 is recruited to IAMs prior to BCV rupture/disassembly, a process known to require T3SS secreted *Shigella* effectors. Thus, we investigated if SNX8 localization was also effector dependent. Given the rapid recruitment of SNX8 to IAMs we investigated the impact of the first set of secreted bacterial effector proteins IpgD and IcsB. The *Shigella* phosphatase, IpgD, is involved in the recruitment of PI(3)P to IAMs and mutants have been reported to strongly decrease IAM numbers, with a delay in BCV rupture (Mellouk et al., 2014; Weiner et al., 2016). The effector IcsB, an N-fatty acylase, is known to modify multiple cellular host factors (Liu et al., 2018) and participates in actin cocoon formation (Kühn et al., 2020).

In order to monitor SNX8 dynamics and recruitment, a 2-minute interval microscopy time-course was performed using SNX8-EGFP and mOrange-Galectin-3 co-transfected HeLa cells infected with either wildtype *Shigella* or deletion mutants Δ*icsB* and Δ*ipgD*. Analysis of these time lapse movies showed a notable decrease in the SNX8 positive IAMs surrounding the BCV upon invasion of *Shigella* Δ*ipgD* or Δ*icsB* mutants (Figs. 3**C** and 3**B** respectively) compared to *Shigella* WT infected cells (Fig. 3**A**). To control whether this reduction in SNX8 positive IAMs was due to a defect in SNX8 recruitment or simply a reduction in IAM formation, we performed similar experiments, using the fluorescent fluid phase marker dextran to label total IAMs (Weiner et al., 2016), and fixing the cells 30 min post invasion (Figs. 3**D** and 3**E**). We observed no significant difference in the number of total IAMs and a strong decrease in SNX8-positive compartments between the WT and Δ*icsB* mutant. In the case of infections with the Δ*ipgD* mutant there was a strong reduction in the overall IAM number, indicating that the decline in SNX8-positive macropinosomes can be at least partially explained by the loss of IAMs production by this mutant. Additionally, infections with a *Shigella* Δ*ipaJ* mutant were performed, IpaJ has been shown to cleave the N-myristoyl group of host GTPases Arf1 and Arf2, inhibiting vesicular trafficking (Burnaevskiy et al., 2013; Burnaevskiy et al., 2015). Our result shows that the Δ*ipaJ* mutant have a similar phenotype compared with *Shigella* WT (Supplementary Figure 2), indicating a specificity of the IpgD and IcsB effectors for the recruitment of SNX8 to IAMs.

3.4. SNX8 is recruited to a PI(3)P positive subpopulation of IAMs

We previously showed that a portion of IAMs produced during *Shigella* infections are positive for PI(3)P (Weiner et al., 2016). Interestingly, SNX8 contains a PX domain binding to PI(3)P (Van Weering et al., 2012). We speculated that SNX8 recruitment and PI(3)P presence to IAMs occurred concurrently in time. To address this we performed time-lapse microscopy at 1 min-intervals to capture the *Shigella* infection of HeLa cells transiently co-transfected with SNX8-EGFP and mCherry-2xFYVE- a PI(3)P binding probe construct (Stenmark et al., 1996). Our results showed the localization of 2xFYVE to IAMs occurred simultaneously with EGFP-SNX8 enrichment (Fig. 4**A**). Moreover, to evaluate the percentage of 2xFYVE positive IAMs that also recruit SNX8 we performed infections with *Shigella* WT in cells transfected with 2xFYVE-mCherry and SNX8-EGFP and scored the presence of each marker at 30 min post infection (Fig. 4**E**). Our data shows that the majority of IAMs recruit SNX8 (51.2%), while an important percentage of the total IAMs were positive for both SNX8 and 2xFYVE (30.9%).

How IAMs are involved in the intracellular trafficking of *Shigella* remains unclear, and it is unknown whether all IAMs are of the same composition (Mellouk et al., 2014; Weiner et al., 2016; Chang et al., 2020). To assess whether SNX8 localizes to all *Shigella*-IAMs, we first performed time-lapse microscopy experiments at higher spatial resolution using the LactC2 reporter to carefully monitor IAMs. In brief, 1-minute-interval time-course experiments were performed on LactC2-GFP stable HeLa cells, transiently transfected with SNX8-mApple and infected with *Shigella.* Image analysis confirmed that all IAMs were labelled by LactC2-GFP throughout their lifetime (Fig. 4**B**). Moreover, we also noted that SNX8 recruitment to IAMs begins shortly after IAM cup closure to a subset of the total IAMs formed (Fig. 4**B**). To address this, we performed experiments with either the WT strain or the Δ*ipgD* mutant, using the fluorescent fluid phase marker dextran to label IAMs (Weiner et al., 2016) in SNX8-EGFP transiently transfected HeLa cells that were fixed after 30 min post-infection (Figs. 4**C** and 4**D**). These results further confirmed SNX8 to be enriched only to a subpopulation of the formed IAMs in cells infected with the WT strain. In the case of the Δ*ipgD* mutant, we observed very few IAMs generated by infection focus, as described previously (Mellouk et al., 2014; Weiner et al., 2016; Chang et al., 2020), and the majority were SNX8 negative. Together, these results reveal the co-existence of at least two subsets of IAMs of distinct composition within an infection focus.

3.5. Characterization of SNX8 behavior during IAMs maturation

Previously, several small RAB GTPases were shown to be recruited during *Shigella*-IAM maturation with several of them playing a role in promoting the invasion steps (RAB8A, RAB11A), also marking the importance of IAM-recruited factors (Mellouk et al., 2014; Weiner et al., 2016; Chang et al., 2020). Given the recruitment of SNX8 to IAMs at early stages of infection, we postulated there was a spatial-temporal relationship with the recruitment of Rab GTPases to the IAMs. To address this, we co-transfected SNX8 and RAB5A, RAB7A, RAB8A or RAB11A and performed time-lapse microscopy at 35 s-interval to temporally resolve the precise recruitment of these different factors.

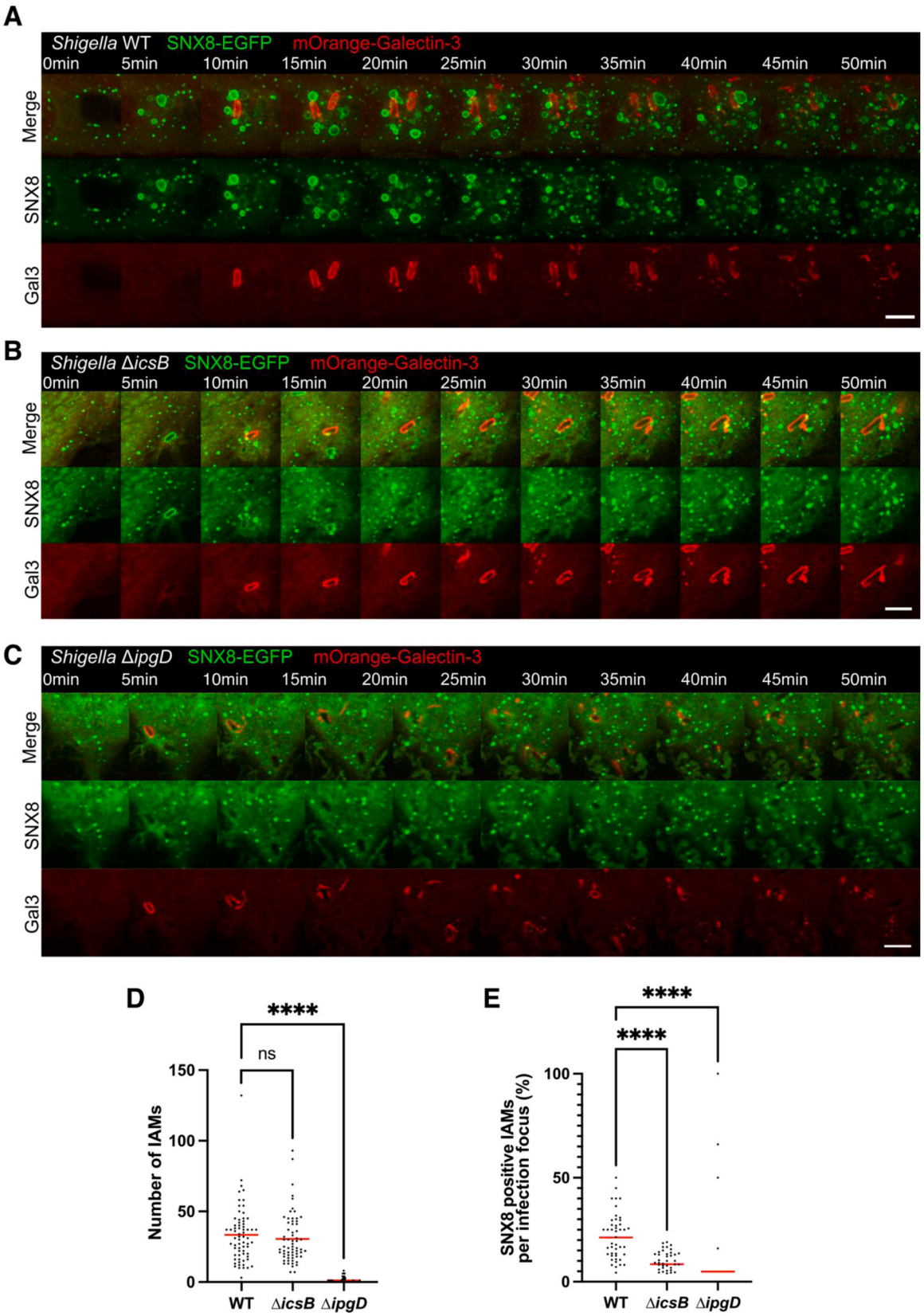

Fig. 3. SNX8 recruitment to the *Shigella* infection site is impacted by the bacterial effectors IpgD and icsB. HeLa cells co-expressing SNX8-EGFP (in green) and mOrange-Galectin-3 (in red) were infected with either *Shigella* WT (**A**) or the mutants Δ*ipgD* (**B**) and Δ*icsB* (**C**). Galectin-3 signal indicates the moment of BCV rupture and labels the ruptured BCV membrane-remnants. The infection start (t = 0) was defined by the first apparition of membrane ruffles. Scale bar is 5 μm. Quantification of total (**E**) or SNX8-positive (**F**) IAMs in HeLa cells expressing SNX8-EGFP and infected with *Shigella* WT or mutants expressing dsRed together with dextran-alexa647 and fixed 30 min after infection. The analysis was performed on 3 biological replicates (n > 45 infection foci per condition).

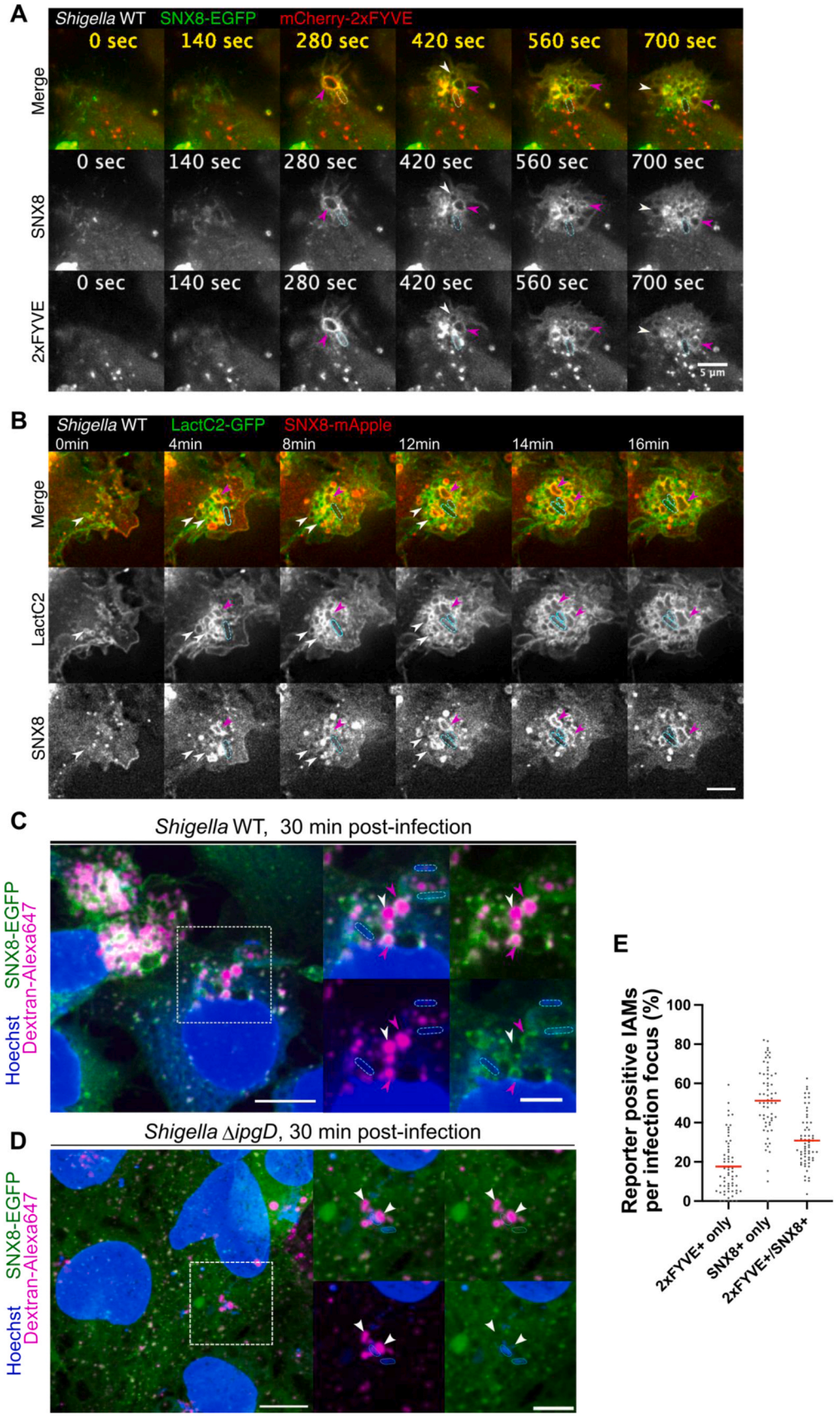

(caption on next page)

Fig. 4. SNX8 is heterogeneously recruited to IAMs and partially co-localizes with PI(3)P. Time-lapse microscopic analysis of SNX8 distribution at IAMs by transfecting SNX8-mApple in (**A**) cells co-transfected with 2xFYVE-EGFP or (**B**) LactC2-GFP-expressing HeLa cells. Entering bacteria are tracked with cyan outlines. Magenta and white arrowheads highlight SNX8 positive and negative IAMs respectively. The infection start (t = 0) was defined by the first apparition of membrane ruffles. Scale bar is 5 μm. **C,D**. Fixed confocal image of HeLa cells expressing SNX8-EGFP and infected with *Shigella* WT or *ΔipgD* together with dextran-Alexa647 at 30 min post-infection. SNX8 signal is in green and dextran-containing IAMs are in magenta. Magenta arrowheads show SNX8 positive-IAMs, white arrowheads show SNX8 negative IAMs and in cyan is outlined the bacteria. Inset show: a zoomed merged image with all channels (top left panel). The top right panel shows the SNX8-EGFP (in green) localizing to part of the IAMs formed (in magenta). Bacteria (outlined) together with IAMs are shown in the bottom left panel and an overview to the SNX8-EGFP recruitment on the bottom right panel. Scale bars are 10 μm and 5 μm. **E**. Quantification of IAMs recruiting SNX8-mApple and/or 2xFYVE-EGFP following 30 min of infection with WT *Shigella*. The average percentage of IAMs recruiting each reporter per infection foci is shown and the median is displayed (2xFYVE positive: 17.6%, SNX8 positive: 51.2%, double positive: 30.9%). The analysis was performed in two biological replicates (n > 60 infection foci per condition).

Canonical macropinosome maturation has previously been reported to involve the early marker RAB5A and late marker RAB7A (Egami et al., 2014; Buckley and King, 2017). Our data showed recruitment of RAB5A to IAMs early on during the *Shigella* invasion process as previously reported by Mellouk et al. (2014) (Fig. 5**A**). Microscopy time-lapse images showed SNX8 recruitment occurs simultaneously with RAB5A recruitment to IAMs (Figs. 5**A** and 5**B**). Furthermore, temporal analysis of SNX8 and RAB5A fluorescence intensity to individual IAMs further emphasized this observation (see Fig. 5**B**). Microscopic analysis also revealed SNX8 recruitment to IAMs occurred prior to RAB7A accumulation and decreased with RAB7A presence (Figs. 5**C** and 5**D**). Moreover, nearly all SNX8-IAMs acquired RAB7A and we observed formation of SNX8-negative RAB7A-positive tubules suggesting distinct recycling pathways of RAB7 and SNX8. These results show SNX8 recruitment to occur in "canonical macropinosome"-like maturing IAMs as soon as the early stage of IAMs maturation and it remains present until later stages of IAM maturation.

RAB11A and RAB8A enrichment to IAMs was found to promote efficient BCV rupture and egress (Weiner et al., 2016; Chang et al., 2020). Therefore, we wanted to compare SNX8 recruitment with these factors. Analysis of the time-lapse images showed that in the case of RAB11A and RAB8A overexpression, SNX8 was only partially recruited to the formed IAMs (Figs. 5**E** and 5**G**). We distinguished in both cases 3 distinct recruitments: (i) the recruitment of both overexpressed proteins, (ii) recruitment of the RAB protein only and (iii) an exclusive SNX8 recruitment. For IAMs that showed recruitment of both host factors, we observed RAB8A recruitment to IAMs prior to SNX8 recruitment (Figs. 5**E** and 5**F**), however these factors did not seem to overlap at the monitored IAMs. When co-expressing RAB11A and SNX8, SNX8 was recruited first to IAMs and was then replaced by RAB11A (Fig. 5**G**). Analysis of individual IAMs also showed this switch (Fig. 5**H**). Interestingly, when overexpressing dominant negative (DN) or constitutively active (CA) versions of RAB11, we could observe a longer residence time of SNX8 at the IAM membranes (Supplementary Figure 3). This hints that a functional RAB11 GTPase activity is required for SNX8 removal from these compartments. Altogether, our time-resolved data shows distinct profiles of SNX8 positive IAMs with individual Rab GTPases. Overall, these results show SNX8 recruitment is mutually exclusive to RAB11A and RAB8A at IAMs and this hints at the existence of divergent IAM subpopulations during *Shigella* infection.

3.6. SNX8/PI(3)P impairment to IAMs hampered Shigella BCV egress

We proceeded to investigate the function of this newly identified subset of PI(3)P + /SNX8 + IAMs to determine their impact on BCV rupture. We first assessed whether this process required the host-cell PI (3)-kinase. This was confirmed by using the broad spectrum PI(3)-kinase inhibitor wortmannin (Supplementary Figure 4), which led to an arrest of SNX8 recruitment to IAMs. We remarked however that SNX8 recruitment to the BCV remained, implying a PI(3)-kinase independent recruitment to this bacterial compartment.

Given the PI(3)P-dependent recruitment of SNX8 together with RAB5A, we reasoned that the RAB5 effector class III PI(3)P kinase VPS34 (Vacuolar Protein Sorting 34) could be involved as it has a reported role in early endosome and macropinosome PI(3)P maturation (Bohdanowicz et al., 2013; Spangenberg et al., 2021). To test this hypothesis, we used the VPS34-specific inhibitor SAR405, which has been described to impair VPS34 function in canonical macropinosomes (Ronan et al., 2014; Spangenberg et al., 2021). Therefore, we performed time-lapse infections in HeLa cells transiently expressing mOrange-Galectin-3 and SNX8-eGFP with and without SAR405. We observed that addition of SAR405 hampered the recruitment of SNX8-eGFP to IAMs (Figs. 6**A and** 6**B**) but did not impact bacterial invasion (Supplementary Figure 4). The inhibitor also impaired PI(3)P-recruitment to IAMs, but did not fully abolish the presence of PI(3)P at the BCV (Supplementary Figure 4).

Given the dynamics of SNX8 recruitment in relationship to IAM formation during *Shigella* intracellular niche formation, we examined if SNX8 positive IAMs are involved in BCV rupture or in other steps of BCV disassembly. To track the BCV rupture and membrane remnants, we performed time lapse infections of SAR405 treated HeLa cells co-expressing SNX8-eGFP together with the fluorescent reporter mOrange-Galectin-3. BCV rupture time was defined as the time in between membrane ruffling and Galectin-3 recruitment to the BCV (see illustration in Fig. 6**C**). Analysis of the BCV rupture time showed a slight, yet significant delay in the presence of the SAR405 inhibitor compared to the DMSO control (Fig. 6**C**).

To monitor unpeeling of BCV membrane remnants, we were able to discern three phenotypes on the basis of BCV membrane movement and the swiftness of bacterial movement: we distinguish a quick BCV disassembly, loose BCV remnants leading to a rapid onset of *Shigella* motility, and tight BCV remnants with delayed intracellular *Shigella* motility (see Fig. 6**D**). Quantification of these phenotypes is in agreement with previously reported proportions of each type of BCV disassembly in the presence of DMSO (Kühn et al., 2020) with tight BCV remnants: 44.2%, loose BCV remnants: 40.5% and quick recycling: 15.4% (Fig. 6**D**). We observed no change in the quick BCV disassembly phenotype in the presence of the VPS34 inhibitor (DMSO=15.2%, SAR405 =15.7%,). However, the addition of the VPS34 inhibitor resulted in a shift in the efficiency of BCV disassembly (Fig. 6**D**). Here, only 34% of infected cells were able to disassemble the BCV remnants efficiently, while 50% remained trapped within BCV remnants. Moreover, we performed infections in the presence of dextran to evaluate the effect of SAR405 on the subset of SNX8 + IAMs and the total number of IAMs (Fig. 6**E-F**). At 30 min pi, there is a significant decrease in the number of SNX8 + IAMs upon treatment with SAR405 (Fig. 6**G**), while there is no difference in the number of total IAMs between control and treated cells (Fig. 6**H**). Together, these results indicate a contribution of this specific subtype of IAMs (PI(3)P + /SNX8 +) in promoting efficient *Shigella* BCV egress to reach the host cytosol.

3.7. SNX8 depletion leads to faster Shigella BCV release

Finally, to assess the role of SNX8 at the IAMs independently from the presence of PI(3)P, we performed infections in cells transfected with siRNA against SNX8 or control and monitored the BCV rupture and unpeeling time (Fig. 7). Depletion of SNX8 in HeLa cells led to a faster vacuolar rupture (control-siRNA 7.6 min v/s siRNA-SNX8 6.2 min) (Fig. 7**C**). Moreover, the effect on the time it took for the BCV to unpeel

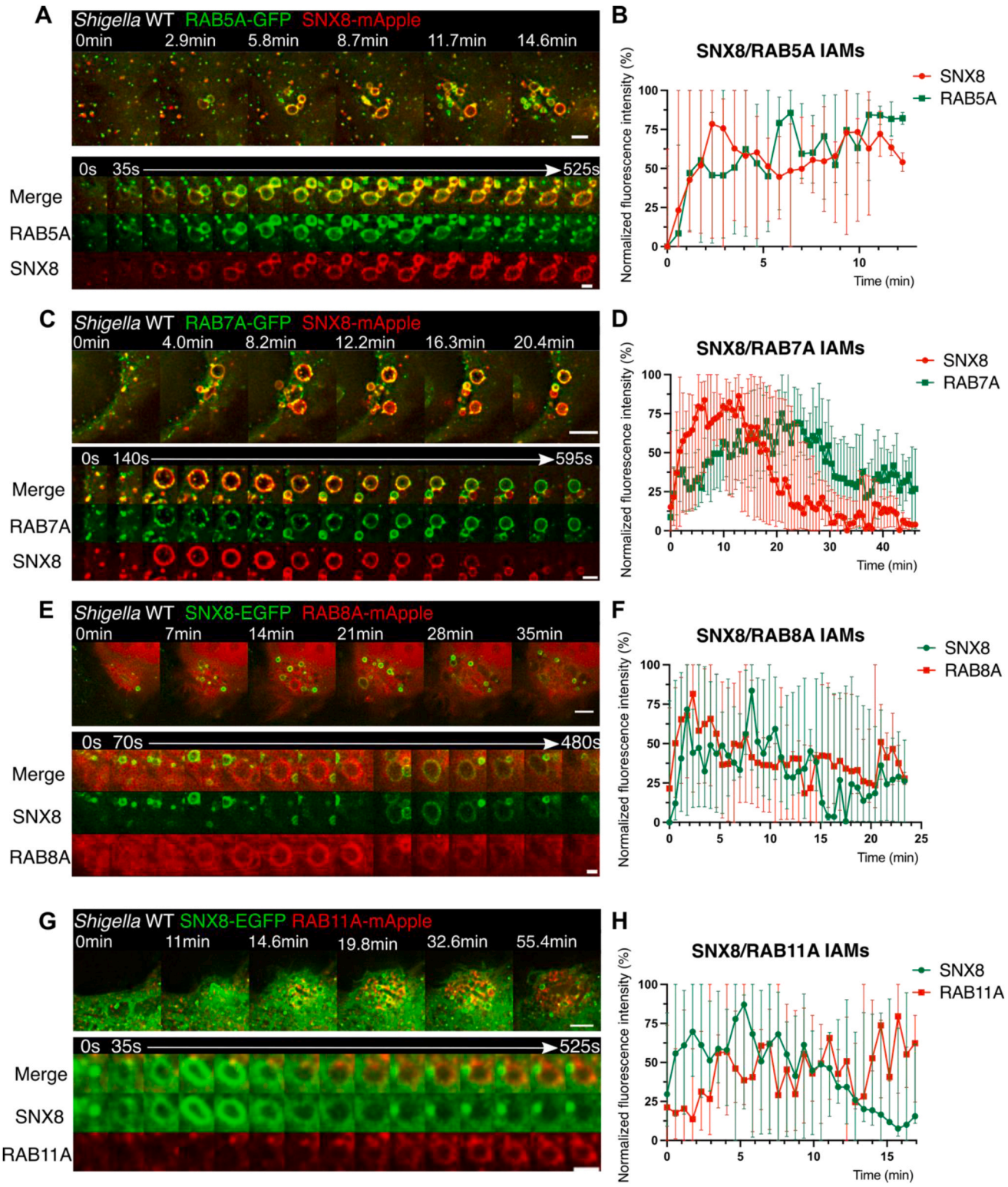

Fig. 5. Characterization of the maturation of SNX8-IAMs to RAB GTPases. Live cell 35 s time-lapse microscopy images of HeLa cells co-expressing RAB GTPases and SNX8 and infected with *Shigella*: **A**. RAB5A-GFP/SNX8-mApple, **C**. RAB7A-GFP/SNX8-mApple, **E**. SNX8-EGFP/RAB8A-mApple, **G**. SNX8-EGFP/RAB11A-mApple. The infection foci and a zoom on a macropinosome of the infection site are shown together. Scale bars are 3 μm and 1.5 μm, respectively. **B**. Normalized fluorescence intensity of SNX8-mApple and RAB5A-GFP to individual IAMs (n = 8 events). **D**. Normalized fluorescence intensity of SNX8-mApple and RAB7A-GFP to individual IAMs (n = 8 events). **F**. Normalized fluorescence intensity of SNX8-EGFP and RAB8A-mApple to individual IAMs (n = 6 events). **H**. Normalized fluorescence intensity of SNX8-EGFP and RAB11A-mApple to individual IAMs (n = 8 events). In all cases, fluorescence intensity was normalized to the maximum and minimum intensities measured for each individual IAM. Error bars: standard deviation. Dots represent average normalized fluorescence intensities at the IAMs membranes, for each time point and solid lines the interpolation of the signal evolution between each time point.

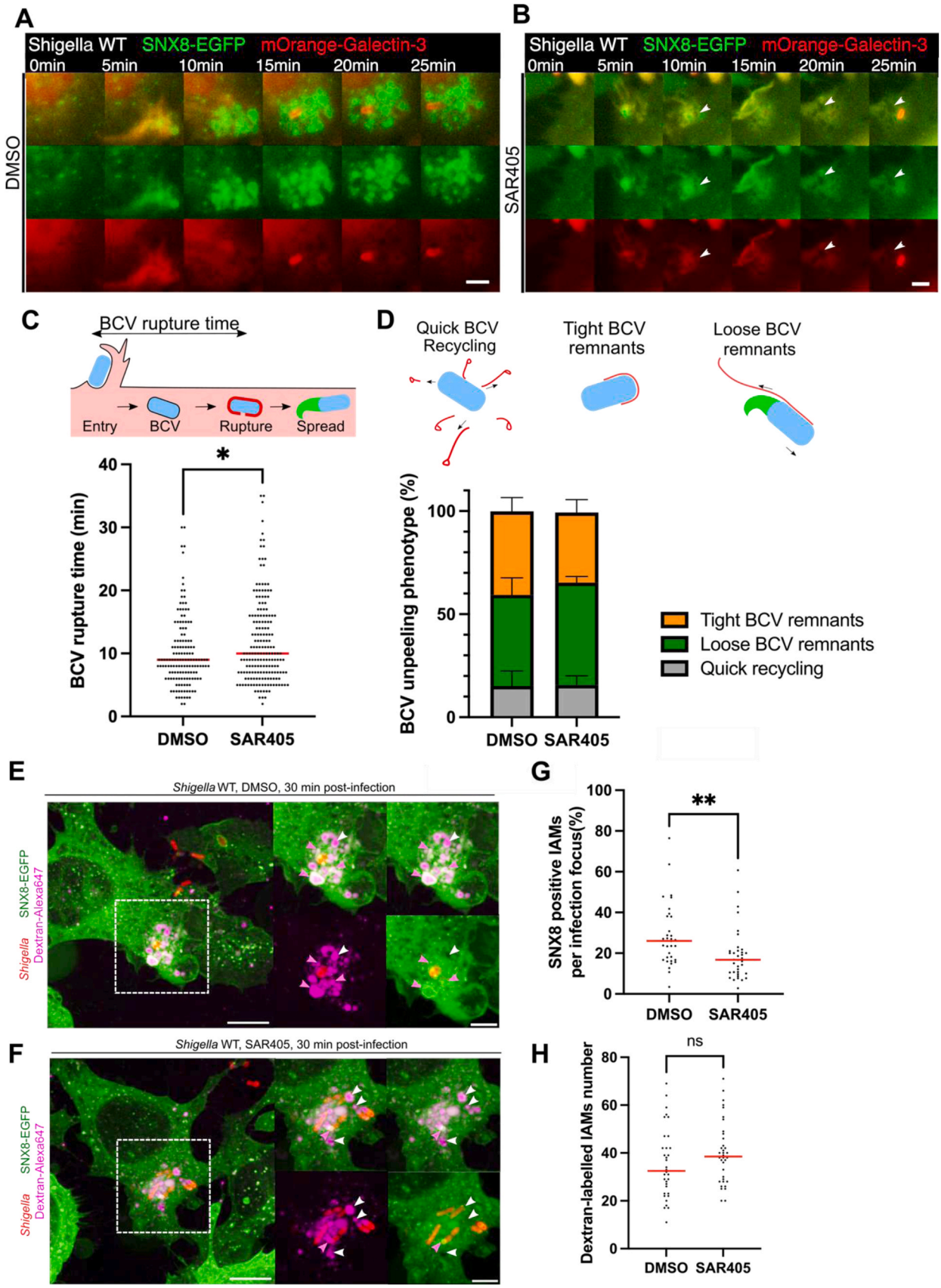

(caption on next page)

Fig. 6. SNX8-PI(3)P IAMs promote BCV rupture and rapid bacterial escape from the BCV. A, B. Time-lapse images of *Shigella* infections in SNX8-eGFP/mOrange-Galectin-3 transiently transfected HeLa cells in the presence of DMSO or SAR405 inhibitor. White arrowheads show SNX8-negative IAMs. Scale bar is 5 μm. **C.** BCV rupture time of the first 3 bacteria entering a bacterial focus in WT *Shigella* infected cells in the presence of DMSO or SAR405 (n > 140 events for each condition). Statistical analysis was performed using an unpaired t-test (* $P < 0.05$). **D.** Quantification of BCV unpeeling events in SNX8-EGFP and mOrange-Galectin-3 expressing HeLa cells treated with SAR405 or DMSO (nDMSO=233, nSAR405 =289). Schematic illustrations depict the phenotypes analyzed: quick recycling with quick BCV recycling with rapid recycling of the membrane from the bacteria, tight BCV remnants with delayed bacteria movement and loose BCV remnants with bacteria movement. **E, F.** Confocal images of HeLa cells expressing SNX8-EGFP and infected with *Shigella* together with dextran-Alexa647 in the presence of either DMSO or SAR405 inhibitor and fixed 30 min post-infection. White arrowheads show SNX8-negative IAMs and magenta arrowheads show SNX8-positive IAMs. Scale bars are 10 μm and 5 μm. Quantification of SNX8-positive IAMs (**G**) or total number of dextran-positive IAMs (**H**) in the presence of either DMSO or SAR405 inhibitor. The analysis was performed in 3 biological replicates (n > 30 infection foci per condition).

was also decreased significatively (Fig. 7**D**). Quantification of the BCV unpeeling phenotypes showed that, upon SNX8 depletion, more bacteria were able to disassemble the BCV remnants efficiently via loose remnants or quick recycling, with the concomitant decrease in the percentage of bacteria trapped by tight vacuole remains.

In summary, our results indicate that there are macropinosomes of different identities at a given invasion site. These IAM subpopulations exhibit opposing roles, highlighting the interplay between host and bacterial factors that control the timing and efficiency of BCV rupture, unpeeling and cytosolic dissemination.

4. Discussion

Following a comprehensive screen of the involvement of BAR proteins during *Shigella* invasion combining time-resolved fluorescence microscopy with genetically-encoded markers for intracellular bacterial localization (Sanchez et al., 2022), we discovered the existence of distinct *Shigella*-IAM subpopulations. We studied a subset of IAMs which are PI(3)P and SNX8 positive showing their implication in efficient bacterial vacuole egress upon initial BCV breakage. We identified the PI(3)P signal to be VPS34-dependent on the IAMs (in contrast to the BCV), and we showed that at least part of this subset of IAMs underwent a RAB11A switch. Lastly, PI(3)P synthesis arrest to these IAMs shifted the balance of pathogens being trapped within broken BCVs to efficiently disassembled BCVs.

Shigella invasion steps require extensive membrane remodeling. Hence, monitoring BAR domain-containing factors involved in *Shigella* invasion appeared as promising. Previously, TOCA-1 was reported to be recruited to the *Shigella* actin cage and to be crucial for actin-tail formation (Leung et al., 2008; Baxt and Goldberg, 2014; Kühn et al., 2020) which we also observed (data not shown). We found an enrichment of SNX-BAR proteins, in particular SNX8, which is partially localized to PI(3)P positive IAMs and was retained until late *Shigella* invasion steps (Fig. 2). With our data, we could determine the existence of a PI(3)P + /SNX8 + subset of *Shigella*-IAMs (Fig. 4). Our results align with a report from Weiner et al. (2016) which showed PI(3)P-labelled IAMs partially co-localizing with the fluid phase marker dextran. Previously, macropinocytosis was proposed as the entry mechanism for bacterial pathogens (Cossart and Sansonetti, 2004). However, *Shigella*-IAMs were determined to be distinct morphologically and in composition from the bacterial phagosome-like vacuole (Weiner et al., 2016) prompting their formation as being driven by separate mechanisms. Furthermore, contact sites between the BCV and IAMs were reported (Weiner et al., 2016) as well as the recruitment of host factors RAB11A, RAB8A and the exocyst complex (Mellouk et al., 2014; Weiner et al., 2016; Chang et al., 2020) which were revealed to promote *Shigella*-BCV egress. Together these data highlight IAMs as a separate compartment with an important contribution to the infection process. Although morphologically comparable to canonical macropinosomes, the similarity in composition and formation of IAMs to "classical" macropinosomes has remained unclear. A recent study (Spangenberg et al., 2021) found canonical macropinosome maturation to be VPS34-dependent with inhibition of VPS34 leading to the refusion of macropinosomes with the plasma membrane, via RAB10 and RAB11A recruitment. Here, our results contrasted with those of Spangenberg et al. with the VPS34-mediated PI(3)P + /SNX8 + IAMs subset maturing to RAB11A, highlighting how these pathogen-controlled compartments differ from canonical macropinosomes. This suggests there are additional assembly components assembled on these pathogen-controlled compartments which lead to a distinct trafficking outcome in comparison to canonical macropinosomes.

Through our study of the PI(3)P + /SNX8 + subpopulation of IAMs, we can speculate about the potential function(s) and maturation of the different subsets of IAMs. Based on RAB recruitment, we propose that some subsets may follow the RAB7A endosomal degradation pathways, SNX8 + /RAB11A- subsets of IAMs may be subject to communicate with the TGN whereas SNX8-/RAB11A+ IAMs may become "recycling endosome-like" potentially undergoing recycling at the plasma membrane. This work highlights *Shigella* infection foci as being composed of subpopulations of IAMs with potential to subvert multiple host trafficking pathways. This is in agreement with previous studies that demonstrated a function of IAMs in accelerating *Shigella*-BCV egress (Mellouk et al., 2014; Weiner et al., 2016; Chang et al., 2020) and emphasizing both a contribution of the host and the bacteria.

Broadly our work highlights the importance of the endosomal recycling pathways in the later steps of *Shigella* invasion. *Shigella* has been shown to require rapid loss of host membrane remnants to gain access to the host cytosol (Chang et al., 2020; Kühn et al., 2020). BCV egress, has been found to require first the rupture of the BCV followed by the unpeeling of the BCV remnants. Furthermore, BCV unpeeling has been described as impacting the capacity of the bacteria to move within cells and into neighboring cells (Kühn et al., 2020; Chang et al., 2020). It is likely that the efficiency of these events impact on intracellular detection by xenophagy (Wandel et al., 2017). We show in this study that IAMs play a role in the shedding of the BCV membrane from the bacteria. However, we show here that *Shigella* triggers maturation of different IAMs subsets with different trafficking pathways that may contribute to additional aspects of the infection process. Moreover, we could detect within the same invasion foci IAMs of different identities, at the lipid and protein level. The different IAM subsets appeared to play opposite roles with regards to the vacuolar rupture process. Possibly, this reflects the complex dynamic interplay of host and bacterial factors involved during *Shigella* cytosolic escape. Maturation defects of the BCV could be previously detected monitoring the invasion of different *Shigella* mutants including Δ*icsB* (Kühn et al., 2020). Δ*icsB*-dependent reduction in SNX8-positive IAMs did not correlate with a faster rupture of the vacuole suggesting that IpgB acted through different pathways on the IAMs and other cellular processes, such as the formation of the actin cage around intact BCVs.

The bacterial factors that dictate the diversity of IAMs during *Shigella* entry need to be determined. The Δ*ipgD* mutant leads to a slight delay in bacterial entry, however it almost entirely abrogated the formation of IAMs (Garza-Mayers et al., 2015; Weiner et al., 2016). These studies together with our data using the PI(3)P kinase inhibitors suggest it is unlikely that IpgD is key to controlling the different IAM subsets. Interestingly, another effector has been shown to modulate small host GTPases. IcsB is an N-fatty acylase that covalently binds small GTPases to host membranes during *Shigella* invasion (Liu et al., 2018). We have also found that it is involved in the formation of the actin cocoon, and it has an impact on egress of *Shigella* from its vacuole (Kühn et al., 2020).

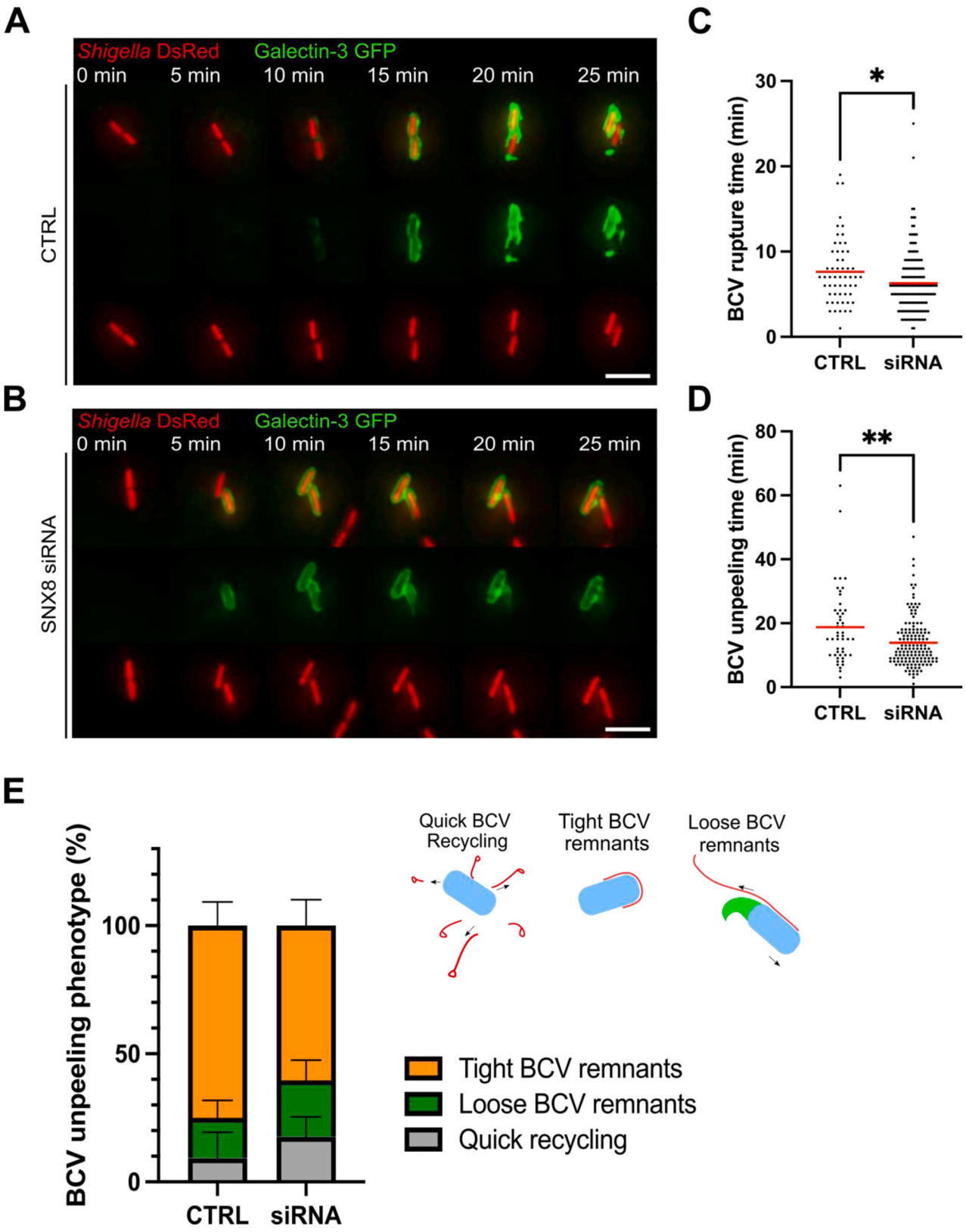

Fig. 7. SNX8 depletion reduces BCV rupture time and BCV unpeeling. A, **B**. Time-lapse images of *Shigella* infections in GFP-Galectin-3 HeLa cells transfected with siRNA control or against SNX8. Scale bar is 5 μm. **C**. BCV rupture time of the first 3 bacteria entering a bacterial focus (nCTRL=56, nsiRNA=171). **D**. Quantification of BCV unpeeling time of GFP-Galectin-3 expressing HeLa cells transfected with siRNA control or against SNX8 and infected with *Shigella* WT (nCTRL=49, nsiRNA=149). **E**. Quantification of BCV unpeeling phenotypes (nCTRL=51, nsiRNA=142). Schematic illustrations depict the phenotypes analyzed: quick recycling with quick BCV recycling with rapid recycling of the membrane from the bacteria, tight BCV remnants with delayed bacteria movement and loose BCV remnants with bacteria movement. All analysis were performed in 3 biological replicates. Statistical analysis were performed using an unpaired *t*-test (* $P < 0.05$, ** $P < 0.01$).

Therefore, it would be interesting to study how the Δ*icsB* mutant affects the different subpopulations of IAMs. Furthermore, IpaB and IpaJ have been identified to be involved in Golgi fragmentation, and it is possible that these pathways also regulate the various subsets of IAMs (Burnaevskiy et al., 2013).

Other bacterial pathogens have also been described to trigger macropinosome-like compartments during their invasion. In particular, *Salmonella* -a bacterial pathogen closely resembling *Shigella*- has been shown to form IAMs during infection. Recently, these *Salmonella*-IAMs were shown to be critical for *Salmonella* niche establishment (Stévenin et al., 2019). IAMs were shown to fuse to the *Salmonella* vacuole, forming the *Salmonella* replicative niche (90% of events), whereas impairment of IAM fusion lead to rupture of the *Salmonella* vacuole (Perrin et al., 2004; Malik-Kale et al., 2012; Knodler et al., 2014). Hence, a comparison of the composition of *Salmonella*-IAMs and *Shigella*-IAMs is crucial to understanding bacteria niche establishment. This could help to highlight specific pathways exploited by bacterial pathogens to establish their intracellular niche.

SNX-BAR proteins have been previously shown to be important targets for invasive bacteria. The *Chlamydia* "inclusion", the pathogen's replicative niche, was reported to selectively recruit SNX5, SNX6 and SNX32 through the *Chlamydia* effector IncE. These were shown to form tubules at this compartment and to be crucial for Chlamydia replication within its host (Mirrashidi et al., 2015; Elwell et al., 2017; Paul et al., 2017). *Salmonella,* a bacterium residing within a replicative niche called the *Salmonella*-containing vacuole (SCV), has also been reported to reprogram SNX-BAR proteins. *Salmonella* has been shown to hijack SNX-18 for its entry within the host cell (Liebl et al., 2017) and once internalized, *Salmonella* induces SNX recruitment to the SCV through the *Salmonella* effector SopB-mediated by PI(3)P formation (Stévenin et al., 2019). Similar to *Chlamydia*, SNX1 forms tubules at the SCV which have been shown to regulate bacterial niche establishment (vacuole stability or rupture). SNX-BAR subversion has also been reported in a cytosol-residing bacterium. Through the oral listeriosis enhancing effector Lmo1656, *Listeria* has been described to recruit SNX6 for successful *Listeria* infection (David et al., 2018). Altogether these discoveries highlight that SNX-BAR proteins have an important role for membrane remodeling during bacterial invasion across multiple species. From this it is clear that further studies to define how these proteins influence pathogenesis at the host-microbe interface are needed, as they may represent a potentially novel target to prevent bacterial niche establishment.

Funding

JE acknowledges the support from the European Union (ERC-CG-grant: EndoSubvert), and the ANR (program: HBPSensing and PureMagRupture). JE is part of the IBEID and the Milieu Interieur LabExes. The funders had no role in study design, data collection and analysis, decision to publish, or preparation of the manuscript.

CRediT authorship contribution statement

Lensen Arthur: Data curation, Formal analysis, Investigation, Methodology, Validation, Writing – review & editing. **Sanchez Lisa:** Data curation, Formal analysis, Investigation, Methodology, Visualization, Writing – original draft. **Enninga Jost:** Conceptualization, Funding acquisition, Methodology, Project administration, Supervision, Writing – original draft, Writing – review & editing. **Valenzuela Camila:** Conceptualization, Formal analysis, Investigation, Supervision, Validation, Visualization, Writing – original draft, Writing – review & editing. **Hamon Mélanie:** Funding acquisition, Supervision, Writing – review & editing. **Connor Michael G.:** Data curation, Investigation, Resources, Writing – review & editing.

Declaration of Competing Interest

The authors have no conflict of interest.

Acknowledgments

We would like to thank Emmanuel Boucrot for the BAR-domain plasmid library, and to Harald Stenmark, Bruno Goud and Arnaud Echard for sharing molecular tools. We would also like to thank Magdalena Gil for feedback on this manuscript and Yuen-Yan Chang, Laura Barrio-Cano and Sonja Kühn for fruitful discussion on this project. We thank Laurent Audry for technical support. We thank Sandrine Schmutz of (UTechS Cytometry and Biomarkers) of C2RT for technical assistance during cell sorting.

Appendix A. Supporting information

Supplementary data associated with this article can be found in the online version at doi:10.1016/j.ejcb.2023.151381.

References

Baxt, L.A., Goldberg, M.B., 2014. Host and bacterial proteins that repress recruitment of LC3 to *Shigella* early during infection. Apr 10 PLoS One 9 (4), e94653. https://doi.org/10.1371/journal.pone.0094653.

Blocker, A.J., Gounon, P., Larquet, E., Niebuhr, K., Cabiaux, V., Parsot, C., Sansonetti, P. J., 1999. The Tripartite Type III Secreton of *Shigella flexneri* Inserts Ipab and Ipac into Host Membranes. J. Cell Biol. 147, 683–693. https://doi.org/10.1083/JCB.147.3.683.

Bohdanowicz, M., Schlam, D., Hermansson, M., Rizzuti, D., Fairn, G.D., Ueyama, T., Somerharju, P., Du, G., Grinstein, S., 2013. Phosphatidic acid is required for the constitutive ruffling and macropinocytosis of phagocytes. S1-7 Mol. Biol. Cell. Jun. 24 (11), 1700–1712. https://doi.org/10.1091/mbc.E12-11-0789.

Buckley, C.M., King, J.S., 2017. Drinking problems: mechanisms of macropinosome formation and maturation. FEBS J. 284 (22), 3778–3790. https://doi.org/10.1111/febs.14115.

Bujny, M.V., Ewels, P.A., Humphrey, S., Attar, N., Jepson, M.A., Cullen, P.J., 2008. Sorting nexin-1 defines an early phase of *Salmonella*-containing vacuole-remodeling during *Salmonella* infection. J. Cell Sci. 121 (12), 2027–2036. https://doi.org/10.1242/jcs.018432.

Burnaevskiy, N., Fox, T.G., Plymire, D.A., Ertelt, J.M., Weigele, B.A., Selyunin, A.S., Way, S.S., Patrie, S.M., Alto, N.M., 2013. Proteolytic elimination of N-myristoyl modifications by the *Shigella* virulence factor IpaJ. Nature 496 (7443), 106–109. https://doi.org/10.1038/nature12004.

Burnaevskiy, N., Peng, T., Reddick, L.E., Hang, H.C., Alto, N.M., 2015 2. Myristoylome profiling reveals a concerted mechanism of ARF GTPase deacylation by the bacterial protease IpaJ. Mol. Cell 58 (1), 110–122. https://doi.org/10.1016/j.molcel.2015.01.040.

Chan Wah Hak, L., Khan, S., Di Meglio, I., Law, A.L., Lucken-Ardjomande Häsler, S., Quintaneiro, L.M., Ferreira, A., Krause, M., McMahon, H.T., Boucrot, E., 2018. FBP17 and CIP4 recruit SHIP2 and lamellipodin to prime the plasma membrane for fast endophilin-mediated endocytosis. Nat. Cell Biol. 20 (9), 1023–1031. https://doi.org/10.1038/s41556-018-0146-8.

Chang, Y.Y., Stévenin, V., Duchateau, M., Giai Gianetto, Q., Hourdel, V., Rodrigues, C.D., Matondo, M., Reiling, N., Enninga, J., 2020. *Shigella* hijacks the exocyst to cluster macropinosomes for efficient vacuolar escape. PLoS Pathog. 16 (8), e1008822 https://doi.org/10.1371/journal.ppat.1008822.

Cossart, P., Roy, C.R., 2010. Manipulation of host membrane machinery by bacterial pathogens. Curr. Opin. Cell Biol. 22 (4), 547–554. https://doi.org/10.1016/j.ceb.2010.05.006.

Cossart, P., Sansonetti, P.J., 2004. Bacterial invasion: the paradigms of enteroinvasive pathogens. Science 304 (5668), 242–248. https://doi.org/10.1126/science.1090124.

David, D.J., Pagliuso, A., Radoshevich, L., Nahori, M.A., Cossart, P., 2018. Lmo1656 is a secreted virulence factor of *Listeria monocytogenes* that interacts with the sorting nexin 6–BAR complex. J. Biol. Chem. 293 (24), 9265–9276. https://doi.org/10.1074/jbc.RA117.000365.

Dyve, A.B., Bergan, J., Utskarpen, A., Sandvig, K., 2009. Sorting nexin 8 regulates endosome-to-Golgi transport. Biochem. Biophys. Res. Commun. 390 (1), 109–114. https://doi.org/10.1016/j.bbrc.2009.09.076.

Egami, Y., Taguchi, T., Maekawa, M., Arai, H., Araki, N., 2014. Small GTPases and phosphoinositides in the regulatory mechanisms of macropinosome formation and maturation. Sep 30 Front Physiol. 5, 374. https://doi.org/10.3389/fphys.2014.00374.

Elwell, C.A., Czudnochowski, N., von Dollen, J., Johnson, J.R., Nakagawa, R., Mirrashidi, K., Krogan, N.J., Engel, J.N., Rosenberg, O.S., 2017. Chlamydia interfere with an interaction between the mannose-6-phosphate receptor and sorting nexins to counteract host restriction. Mar 2 eLife 6, e22709. https://doi.org/10.7554/eLife.22709.

Garza-Mayers, A.C., Miller, K.A., Russo, B.C., Nagda, D.V., Goldberg, M.B., 2015. *Shigella flexneri* regulation of ARF6 activation during bacterial entry via an IpgD-mediated positive feedback loop. MBio 6 (2), e02584-14. https://doi.org/10.1128/mBio.02584-14.

Jarsch, I.K., Daste, F., Gallop, J.L., 2016. Membrane curvature in cell biology: An integration of molecular mechanisms. J. Cell Biol. 214 (4), 375–387. https://doi.org/10.1083/jcb.201604003.

Jeong, J.Y., Yim, H.S., Ryu, J.Y., Lee, H.S., Lee, J.H., Seen, D.S., Kang, S.G., 2012. One-step sequence-and ligation-independent cloning as a rapid and versatile cloning method for functional genomics studies. Appl. Environ. Microbiol. 78 (15), 5440–5443. https://doi.org/10.1128/AEM.00844-12.

Kim, J.Y., Kim, S.H., Jeon, S.M., Park, M.S., Rhie, H.G., Lee, B.K., 2008. Resistance to fluoroquinolones by the combination of target site mutations and enhanced expression of genes for efflux pumps in *Shigella flexneri* and *Shigella sonnei* strains isolated in Korea. Clin. Microbiol. Infect. 14 (8), 760–765. https://doi.org/10.1111/j.1469-0691.2008.02033.x.

Knodler, L.A., Nair, V., Steele-Mortimer, O., 2014. Quantitative assessment of cytosolic *Salmonella* in epithelial cells. Jan 6 PLoS One 9 (1), e84681. https://doi.org/10.1371/journal.pone.0084681.

Kowarz, E., Löscher, D., Marschalek, R., 2015. Optimized Sleeping Beauty transposons rapidly generate stable transgenic cell lines. Biotechnol. J. 10 (4), 647–653. https://doi.org/10.1002/biot.201400821.

Kühn, S., Bergqvist, J., Gil, M., Valenzuela, C., Barrio, L., Lebreton, S., Zurzolo, C., Enninga, J., 2020. Actin assembly around the *Shigella*-containing vacuole promotes successful infection. Cell Rep. 31 (6), 107638 https://doi.org/10.1016/j.celrep.2020.107638.

Leung, Y., Ally, S., Goldberg, M.B., 2008. Bacterial actin assembly requires TOCA-1 to relieve N-WASP autoinhibition. Cell host Microbe 3 (1), 39–47. https://doi.org/10.1016/j.chom.2007.10.011.

Liebl, D., Qi, X., Zhe, Y., Barnett, T.C., Teasdale, R.D., 2017. SopB-Mediated Recruitment of SNX18 Facilitates *Salmonella* Typhimurium Internalization by the Host Cell. Jun 15 Front Cell Infect. Microbiol 7, 257. https://doi.org/10.3389/fcimb.2017.00257.

Liu, W., Zhou, Y., Peng, T., Zhou, P., Ding, X., Li, Z., Zhong, H., Xu, Y., Chen, S., Hang, H. C., Shao, F., 2018. Nε-fatty acylation of multiple membrane-associated proteins by *Shigella* IcsB effector to modulate host function. Nat. Microbiol. 3 (9), 996–1009. https://doi.org/10.1038/s41564-018-0215-6.

Mahbubur, R., Shoma, S., Rashid, H., El Arifeen, S., Baqui, A.H., Siddique, A.K., Nair, G. B., Sack, D.A., 2007. Increasing spectrum in antimicrobial resistance of *Shigella* isolates in Bangladesh: resistance to azithromycin and ceftriaxone and decreased susceptibility to ciprofloxacin. J. Health, Popul., Nutr. 25 (2), 158.

Malik-Kale, P., Winfree, S., Steele-Mortimer, O., 2012. The bimodal lifestyle of intracellular *Salmonella* in epithelial cells: replication in the cytosol obscures defects in vacuolar replication, 2012 PLoS One 7 (6), e38732. https://doi.org/10.1371/journal.pone.0038732.

McMahon, H.T., Gallop, J.L., 2005. Membrane curvature and mechanisms of dynamic cell membrane remodeling. Nature 438 (7068), 590–596. https://doi.org/10.1038/nature04396.

Mellouk, N., Enninga, J., 2016. Cytosolic access of intracellular bacterial pathogens: the *Shigella* paradigm, 2016 Apr 5 Front. Cell. Infect. Microbiol. 6, 35. https://doi.org/10.3389/fcimb.2016.00035.

Mellouk, N., Weiner, A., Aulner, N., Schmitt, C., Elbaum, M., Shorte, S.L., Danckaert, A., Enninga, J., 2014. *Shigella* subverts the host recycling compartment to rupture its vacuole. Cell Host Microbe 16 (4), 517–530. https://doi.org/10.1016/j.chom.2014.09.005.

Mirrashidi, K.M., Elwell, C.A., Verschueren, E., Johnson, J.R., Frando, A., Von Dollen, J., Rosenberg, O., Gulbahce, N., Jang, G., Johnson, T., Jäger, S., Gopalakrishnan, A.M., Sherry, J., Dunn, J.D., Olive, A., Penn, B., Shales, M., Cox, J.S., Starnbach, M.N., Derre, I., Valdivia, R., Krogan, N.J., Engel, J., 2015. Global Mapping of the Inc-Human Interactome Reveals that Retromer Restricts *Chlamydia* Infection, 2015 Jul 8 Cell Host Microbe 18 (1), 109–121. https://doi.org/10.1016/j.chom.2015.06.004.

Paul, B., Kim, H.S., Kerr, M.C., Huston, W.M., Teasdale, R.D., Collins, B.M., 2017. Structural basis for the hijacking of endosomal sorting nexin proteins by *Chlamydia trachomatis*, 2017 Feb 22 eLife 6, e22311. https://doi.org/10.7554/eLife.22311.

Paz, I., Sachse, M., Dupont, N., Mounier, J., Cederfur, C., Enninga, J., Leffler, H., Poirier, F., Prevost, M.C., Lafont, F., Sansonetti, P., 2010. Galectin-3, a marker for vacuole lysis by invasive pathogens. Cell. Microbiol. 12 (4), 530–544. https://doi.org/10.1111/j.1462-5822.2009.01415.x.

Perrin, A.J., Jiang, X., Birmingham, C.L., So, N.S., Brumell, J.H., 2004. Recognition of bacteria in the cytosol of Mammalian cells by the ubiquitin system, 2004 May 4 Curr. Biol. 14 (9), 806–811. https://doi.org/10.1016/j.cub.2004.04.033.

Peter, B.J., Kent, H.M., Mills, I.G., Vallis, Y., Butler, P.J.G., Evans, P.R., McMahon, H.T., 2004. BAR domains as sensors of membrane curvature: the amphiphysin BAR structure. Science 303 (5657), 495–499. https://doi.org/10.1126/science.1092586.

Puzari, M., Sharma, M., Chetia, P., 2018. Emergence of antibiotic resistant *Shigella* species: a matter of concern. J. Infect. Public Health 11 (4), 451–454. https://doi.org/10.1016/j.jiph.2017.09.025.

Ribet, D., Cossart, P., 2015. How bacterial pathogens colonize their hosts and invade deeper tissues. Microbes Infect. 17 (3), 173–183. https://doi.org/10.1016/j.micinf.2015.01.004.

Ronan, B., Flamand, O., Vescovi, L., Dureuil, C., Durand, L., Fassy, F., Bachelot, M.F., Lamberton, A., Mathieu, M., Bertrand, T., Marquette, J.P., El-Ahmad, Y., Filoche-Romme, B., Schio, L., Garcia-Echeverria, C., Goulaouic, H., Pasquier, B., 2014. A highly potent and selective Vps34 inhibitor alters vesicle trafficking and autophagy, 2014 Dec Nat. Chem. Biol. 10 (12), 1013–1019. https://doi.org/10.1038/nchembio.1681.

Sanchez, L., Chang, Y.Y., Mellouk, N., Enninga, J., 2022. Time-resolved fluorescence microscopy screens on host protein subversion during bacterial cell invasion (Humana, New York, NY). Eff. -Triggered Immun. 113–131. https://doi.org/10.1007/978-1-0716-2449-4_8.

Sansonetti, P.J., Kopecko, D.J., Formal, S.B., 1982. Involvement of a plasmid in the invasive ability of *Shigella flexneri*. Infect. Immun. https://doi.org/10.1128/iai.35.3.852-860.1982.

Schroeder, G.N., Hilbi, H., 2008. Molecular pathogenesis of *Shigella spp.*: controlling host cell signaling, invasion, and death by type III secretion. Clin. Microbiol. Rev. 21 (1), 134–156. https://doi.org/10.1128/CMR.00032-07.

Simunovic, M., Voth, G.A., Callan-Jones, A., Bassereau, P., 2015. When physics takes over: BAR proteins and membrane curvature. Trends Cell Biol. 25 (12), 780–792. https://doi.org/10.1016/j.tcb.2015.09.005.

Simunovic, M., Evergren, E., Callan-Jones, A., Bassereau, P., 2019. Curving cells inside and out: roles of BAR domain proteins in membrane shaping and its cellular implications. Annu. Rev. Cell Dev. Biol. 35, 111–129. https://doi.org/10.1146/annurev-cellbio-100617-060558.

Spangenberg, H., Sneeggen, M., Tortola, M.M., Valenzuela, C., Chang, Y.Y., Stenmark, H., Raiborg, C., Schink, K.O., 2021. A phosphoinositide RAB Switch Controls Early macropinocytosis. https://doi.org/10.1101/2021.11.03.467145.

Stenmark, H., Aasland, R., Toh, B.H., D'Arrigo, A., 1996. Endosomal localization of the autoantigen EEA1 is mediated by a zinc-binding FYVE finger, 1996 Sep 27 J. Biol. Chem. 271 (39), 24048–24054. https://doi.org/10.1074/jbc.271.39.24048.

Stévenin, V., Chang, Y.Y., Le Toquin, Y., Duchateau, M., Gianetto, Q.G., Luk, C.H., Salles, A., Sohst, V., Matondo, M., Reiling, N., Enninga, J., 2019. Dynamic growth and shrinkage of the *Salmonella*-containing vacuole determines the intracellular pathogen niche. Cell Rep. 29 (12), 3958–3973. https://doi.org/10.1016/j.celrep.2019.11.049.

Suarez, A., Ueno, T., Huebner, R., McCaffery, J.M., Inoue, T., 2014. Bin/Amphiphysin/Rvs (BAR) family members bend membranes in cells. Sci. Rep. 4 (1), 1–6. https://doi.org/10.1038/srep04693.

Suzuki, S.W., Oishi, A., Nikulin, N., Jorgensen, J.R., Baile, M.G., Emr, S.D., 2021. A PX-BAR protein Mvp1/SNX8 and a dynamin-like GTPase Vps1 drive endosomal recycling. eLife 10, e69883. https://doi.org/10.7554/eLife.69883.

Swanson, J.A., 2008. Shaping cups into phagosomes and macropinosomes. Nat. Rev. Mol. Cell Biol. 9 (8), 639–649. https://doi.org/10.1038/nrm2447.

Swanson, J.A., 2014. Phosphoinositides and engulfment. Cell. Microbiol. 16 (10), 1473–1483. https://doi.org/10.1111/cmi.12334.

Van Weering, J.R., Verkade, P., Cullen, P.J., 2010. SNX-BAR proteins in phosphoinositide-mediated, tubular-based endosomal sorting, 2010 Jun Semin Cell Dev. Biol. 21 (4), 371–380. https://doi.org/10.1016/j.semcdb.2009.11.009.

Van Weering, J.R., Sessions, R.B., Traer, C.J., Kloer, D.P., Bhatia, V.K., Stamou, D., Carlsson, S.R., Hurley, J.H., Cullen, P.J., 2012. Molecular basis for SNX-BAR-mediated assembly of distinct endosomal sorting tubules, 2012 Nov 28 EMBO J. 31 (23), 4466–4480. https://doi.org/10.1038/emboj.2012.283.

Vanzo, R.J., Martin, M.M., Sdano, M.R., Teta, K., Aggarwal, V., South, S.T., 2014. SNX8: a candidate gene for 7p22 cardiac malformations including tetralogy of fallot. Am. J. Med. Genet. A 164, 554–556. https://doi.org/10.1002/ajmg.a.36242.

Wandel, M.P., Pathe, C., Werner, E.I., Ellison, C.J., Boyle, K.B., von der Malsburg, A., Rohde, J., Randow, F., 2017. GBPs Inhibit Motility of *Shigella flexneri* but Are Targeted for Degradation by the Bacterial Ubiquitin Ligase IpaH9.8. Oct 11 Cell Host Microbe 22 (4), 507–518.e5. https://doi.org/10.1016/j.chom.2017.09.007.

Weiner, A., Mellouk, N., Lopez-Montero, N., Chang, Y.Y., Souque, C., Schmitt, C., Enninga, J., 2016. Macropinosomes are key players in early *Shigella* invasion and vacuolar escape in epithelial cells. PLoS Pathog. 12 (5), e1005602 https://doi.org/10.1371/journal.ppat.1005602.

Weiss, S.M., Ladwein, M., Schmidt, D., Ehinger, J., Lommel, S., Städing, K., Beutling, U., Disanza, A., Frank, R., Jänsch, L., Scita, G., 2009. IRSp53 links the enterohemorrhagic *E. coli* effectors Tir and EspFU for actin pedestal formation. Cell host Microbe 5 (3), 244–258. https://doi.org/10.1016/j.chom.2009.02.003.

Xie, Y., Niu, M., Ji, C., Huang, T.Y., Zhang, C., Tian, Y., Shi, Z., Wang, C., Zhao, Y., Luo, H., Can, D., 2019. SNX8 Enhances Non-amyloidogenic APP Trafficking and Attenuates Aβ Accumulation and Memory Deficits in an AD Mouse. Front. Cell. Neurosci. 13, 410 https://doi.org/10.3389/fncel.2019.00410.

Yi, C.R., Goldberg, M.B., 2009. Enterohemorrhagic *Escherichia coli* raises the I-BAR. Proc. Natl. Acad. Sci. 106 (16), 6431–6432. https://doi.org/10.1073/pnas.0902773106.